RSC Advances

ROYAL SOCIETY OF CHEMISTRY

www.rsc.org/advances

Cite this: DOI: 10.1039/c0xx00000x

www.rsc.org/xxxxxx ARTICLE TYPE

Facile one-pot fabrication of magnetic nanoparticles (MNPs)-supported organocatalysts using phosphonate as an anchor point through direct co-precipitation method

Jingwei Wan, Lu ding, Tao Wu, Xuebing Ma* and Qian Tang

Received (in XXX, XXX) Xth XXXXXXXXX 200X, Accepted Xth XXXXXXXXX 200X
DOI: 10.1039/b000000x

In this paper, a novel type of efficient, magnetically recoverable magnetic nanoparticles (MNPs)-supported 9-amino-9-deoxy-epicinchonidine organocatalysts was prepared through facile co-precipitation method using phosphonic acid (-PO_3H_2) as an anchor point. These MNPs-supported organocatalysts possessed the high and tunable loading capacities of organocatalyst (0.18–0.52 mmol g^{-1}), 2–25 nm regular mesopores and 10.6–44.06 emu g^{-1} saturated magnetization. In the catalytic asymmetric aldol reactions of cyclohexanone with various *o, m* and *p*-substituted benzaldehydes in water, the aromatic aldehydes with the electron-withdrawing substituents including–NO_2, X and -CN afforded the relevant aldol adducts in the excellent yields (86–100%) and steroselectivities (*anti/syn* = 82–98/18–2 and 93–98 %ee *anti*). Especially, the moderate to good yields (36–97%) and steroselectivities (*anti/syn* = 82–96/18–4 and 75–97 %ee *anti*) for the aromatic aldehydes with the strong electron-donating substituents (–CH_3 and –OCH_3) were also satisfactorily achieved. Futhermore, these MNPs-supported organocatalysts could be quantitatively recovered from the reaction mixture by using an external magnet, and reused six times with the excellent catalytic performances (93%, *anti/syn* = 89/11 and 96 %ee *anti*). Meanwhile, MNPs-supported organocatalysts, prepared by surface-modification method, were investigated in detail as comparative samples.

Magnetic nanoparticles (MNPs), which offered many advantages in clean and sustainable chemistry, had been employed superparamagnetic materials as both robust catalysts and catalyst supports because of their easy and efficient recyclability from reaction mixture *via* an external magnet, large surface area, high dispersion and outstanding stability as well as low toxicity and price.[1] In the field of catalysis, these nanostructured catalysts, often metals or metal oxides, served as a bridge between homogeneous and heterogeneous catalysis and acted as a "quasi-homogeneous" or soluble heterogeneous catalysis.[2] There are several protocols for preparing a wide variety of catalytic magnetic recyclable nanocatalysts (MRNCs): silica-based,[3] carbonaceous,[4] polymer-derived [5] and soft functional organic molecule-attached [6] magnetic materials, whose synthetic strategies could be classified into two main families: direct synthesis and template-assisted synthesis. Generally, at least three to five reaction steps were required to obtain MRNCs in template-assisted synthesis, which in the end was tedious, time-consuming and costly. Therefore, in the last two years, some ingeniously designed MRNCs were fabricated through direct synthesis strategy including co-decomposition, impregnation and co-precipitation.[1b, 7]

Asymmetric organocatalysis has blossomed rapidly from infancy to adolescence since the turn of the century.[8] Due to economic consideration, the recycling and reuse of these organocatalysts, including fluorous proline derivatives, solid phase-supported catalysts, ionic liquids, PEG or aqueous media as reaction solvent, is currently a highly sought after goal for our chemists.[9] In the other hand, due to the high loading capacity of catalyst, easy dispersion, outstanding stability, and convenient recycling, MNPs are often used as heterogeneous catalyst supports. However, it was recently reported that MNPs-supported organocatalyst was used as a strategy for the sustainable separation and reuse of chiral organocatalysts. In 2008, S. Luo *et al*. prepared MNP-supported chiral primary amine catalyst by treating SiO_2-MNPs with trimethoxysilane to pave a promising and retrievable way for a range of chiral organocatalysts for the first time.[10] Lately, H. Yang *et al*. covalently grafted L-proline onto SiO_2@Fe_3O_4 nanoparticles.[11] In 2013, Y. Kong *et al*. developed a L-proline-IL-SiO_2@Fe_3O_4-supported organocatalyst for aqueous asymmetric aldol reaction without co-catalyst.[12] In brief, the progress with respect to the application of MNPs in asymmetric organocatalysis only focused on nano Fe_3O_4 coated with silica (SiO_2@Fe_3O_4).

In this paper, in view of the chemical reactivity of phosphonate with ferrous and ferric irons, the one-pot co-precipitation method was introduced to explore a novel type of MNPs-supported organocatalyst with the tunable and controllable loading capacity of chiral organocatalyst using phosphonate (-PO_3H_2) as an anchor point (route 1, **Fig.1**). Meanwhile, MNPs-supported organocatalysts, prepared by surface-modification method, were also investigated in detail as comparative samples (route 2). Based on the

catalytic performances of MNPs-supported organocatalysts in aqueous asymmetric aldol reaction, MNPs-supported organocatalysts by co-precipitation method possessed the higher, more tunable loading capacity of organocatalyst and better catalytic performance than those by surface-modification method. Furthermore, they could be well dispersed in aqueous medium, magnetically recovered from reaction mixture by using an external magnet, and reused six times without significant loss of catalytic activity.

Fig.1 Two routes to MNPs-supported organocatalysts using phosphonate as an anchor point

Experimental

Materials and sample characterization

All chemicals were purchased and used without any further purification. 9-amino-9-deoxy-*epi*-cinchonidine-derived phosphonates **CDPE/n2**, **n4**, **n6** and **CNPE/n4** with different chain lengths (*n*= 2, 4 and 6) were synthesized according to the reference.[13] Fe_3O_4 magnetic nanoparticles (MNPs) with the approximate 80–100 nm diameters were purchased from Aladdin.

Fourier transform infrared spectra were recorded on Perkin–Elmer Model GX Spectrometer using a KBr pellet method with polystyrene as a standard. Thermogravimetric analysis was performed on SBTQ600 thermal analyzer with a heating rate of 20 °C min^{-1} over a temperature range of 40–800 °C under flowing compressed N_2 (100 mL min^{-1}). ^1H, ^{13}C and ^{31}P NMR were performed on a Bruker AV–300 NMR instrument at 300.1, 75.0 and 121.5 MHz, in which all chemical shifts were reported down-field in ppm relative to the hydrogen, carbon and phosphorus resonances of TMS, chloroform-d_1 and H_3PO_4, respectively. The surface morphologies of as-synthesized samples were determined by transmission electron microscope (TEM) and Tecnai G2 F20 (HRTEM) operated at 200 kV. N_2 adsorption-desorption analysis was carried out at 77 K on an autosorb-1 apparatus. The specific surface area and pore diameter were calculated by the BET and BJH model, respectively. X-ray powder diffractions (XRD) were carried out on a XRD-7000 S/L instrument: Cu-Kα radiation, X-ray tube settings of 60kV/80 mA, a step size of 6 ° min^{-1} in the 10–80 ° (2θ) range. The *anti/syn* ratios of aldol products were monitored by ^1H NMR, and their enantiomeric excesses (%ee) were determined on HPLC with a Chiral OD/AD column (*n*-hexane/ 2-propanol = 95/5) under 20 °C, 254 nm and 0.5 mL min^{-1} conditions.

General preparation of chiral organocatalyst containing phosphonic acid

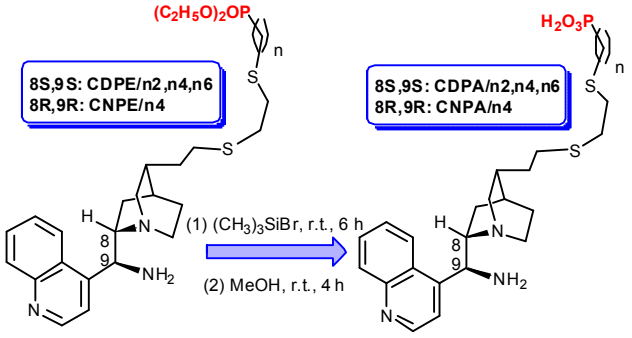

In a flask (100 mL), **CDPE/n4** (0.34 g, 0.4 mmol) and anhydrous CH_2Cl_2 (20 mL) were charged and flushed three times with Ar atmosphere. After being well-mixed, trimethylbromosilane (0.51 mL, 4.0 mmol) was added by a syringe, stirred at room temperature for 6 h and concentrated under reduced pressure. To the residue was added MeOH (20 mL), stirred at room temperature for another 4 h, and then concentrated under reduced pressure to afford viscous yellow solid. The crude product was stirred for 30 min in the deionized water (50 mL), filtered, washed with *n*-pentane (30 mL×4), and dried in vacuo to yield the yellow solid **CDPA/n4** (0.29 g, 91.3%). ^1H, ^{13}C, ^{31}P NMR and MS spectra of **CDPE** and **CDPA** were shown in ESI†.

CDPA/n2: pale yellow solid, m.p. 155-156 °C, δ_H (300 MHz, D_2O, Me_4Si): 9.24 (1H, d, ^3J = 6.0 Hz), 8.65 (1H, d, ^3J = 9.0 Hz), 8.32 (1H, d, ^3J = 9.0 Hz), 8.28 (1H, d, ^3J = 6.0 Hz), 8.22 (1H, t, ^3J = 6.0 Hz), 8.09 (1H, t, ^3J = 6.0 Hz), 5.63 (1H, d, ^3J = 9.0 Hz), 4.37 (1H, d, ^3J = 6.0 Hz), 3.77-3.90 (2H, m), 3.45 (1H, s), 3.17 (1H, d, ^3J = 12.0 Hz), 2.52-2.73 (8H, m), 2.28 (1H, s), 1.69-1.98 (8H, m), 1.11 (1H, s). δ_C (75.0 MHz, $CDCl_3$): 151.9, 145.8, 139.6, 136.6, 132.5, 128.4, 124.9, 123.3, 121.4, 60.6, 56.6, 42.9, 33.4, 32.6, 31.8, 31.7, 29.9, 29.3, 28.2, 25.9, 24.6, 24.4, 24.3. Anal. Calcd for $C_{23}H_{34}N_3O_3PS_2$: C, 55.74; H, 6.91; N, 8.48. Found: C, 55.78; H, 6.90; N, 8.49. MS (ESI+) m/z 495.8 [M+H]+.

CDPA/n4: pale yellow solid, m.p. 155-157 °C, δ_H (300 MHz, D_2O, Me_4Si): 9.14 (1H, d, ^3J = 6.0 Hz), 8.61 (1H, d, ^3J = 9.0 Hz), 8.25 (1H, d, ^3J = 9.0 Hz), 8.08-8.16 (2H, m), 8.01 (1H, t, ^3J = 6.0 Hz), 5.39 (1H, d, ^3J = 9.0 Hz), 4.23 (1H, d, ^3J = 6.0 Hz), 3.72-3.88 (2H, m), 3.34-3.44 (1H, m), 3.11-3.15 (1H, m), 2.45-2.67 (8H, m), 2.25 (1H, s), 1.93-1.95 (3H, m), 1.52-1.79 (9H, m), 1.09 (1H, q, ^3J = 6.0 Hz). δ_C (75 MHz, $CDCl_3$): 153.4, 146.4, 140.9, 135.7, 131.7, 128.1, 124.9, 124.1, 120.9, 61.1, 56.3, 42.6, 33.4, 32.7, 32.0, 32.0, 31.6, 31.0, 30.7, 29.4, 28.8, 27.1, 24.7, 24.5, 24.4. δ_p (121.5 MHz, D_2O, 85% H_3PO_4): 31.1 (s). Anal. Calcd for $C_{25}H_{38}N_3O_3PS_2$: C, 57.34; H, 7.31; N, 8.02. Found: C, 57.30; H, 7.30; N, 8.05. MS (ESI+) *m/z* 523.9 $[M+H]^+$.

CDPA/n6: pale yellow solid, m.p. 160-162 °C, δ_H (300 MHz, D_2O, Me_4Si): 9.21 (1H, s), 8.67 (1H, d, ^3J = 9.0 H), 8.07-8.28 (4H, m), 5.53 (1H, d, ^3J = 9.0 Hz), 4.36 (1H, s), 3.80-3.93 (2H, m), 3.46 (1H, s), 3.22 (1H, s), 2.40-2.62 (8H, m), 2.29 (1H, s), 1.99 (3H, m), 1.14-1.82 (14H, m). δ_C (75.0 MHz, $CDCl_3$): 152.5, 146.6, 140.9, 136.0, 132.1, 128.2, 125.1, 124.2, 121.4, 60.9, 56.4, 42.9, 33.5, 32.9, 32.3, 32.3, 32.2, 30.7, 30.5, 29.7, 29.6, 29.0, 28.6, 27.2, 24.8, 24.6, 23.6. Anal. Calcd for $C_{27}H_{42}N_3O_3PS_2$: C, 58.78; H, 7.67; N, 7.62. Found: C, 58.85; H, 7.70; N, 7.60. MS (ESI+) *m/z* 552.0 $[M+H]^+$.

CNPA/n4: pale yellow solid, m.p. 150-152 °C, δ_H (300 MHz, D_2O, Me_4Si): 9.16 (1H, s), 8.63 (1H, d, ^3J = 9.0 Hz), 8.25 (1H, d, ^3J = 6.0 Hz), 8.06-8.17 (2H, m), 8.03 (1H, t, ^3J = 6.0 Hz), 5.63 (1H, d, ^3J = 9.0 Hz), 4.31 (1H, d, ^3J = 6.0 Hz), 3.38-3.66 (4H, m), 2.37-2.58 (8H, m), 2.19 (1H, s), 1.85-1.91 (3H, m), 1.62-1.67 (1H, m), 1.47-1.52 (8H, m), 1.06-1.17 (1H, m). δ_C (75.0 MHz, $CDCl_3$): 151.7, 148.1, 142.5, 137.0, 133.3, 129.3, 125.9, 125.8, 122.6, 62.5, 51.3, 50.5, 34.0, 33.4, 33.3, 32.9, 32.1, 32.0, 30.5, 29.9, 28.1, 26.2, 25.3, 24.7, 24.2. Anal. Calcd for $C_{25}H_{38}N_3O_3PS_2$: C, 57.34; H, 7.31; N, 8.02. Found: C, 57.31; H, 7.29; N, 7.99.

MS (ESI+) *m/z* 523.9 $[M+H]^+$.

General procedure for MNPs-supported organocatalysts by co-precipitation (Route 1)

The reaction mixture of **CDPA/n4** (130 mg, 0.25 mmol), aqueous $FeCl_2$ solution (4.6 mL, 0.25 mol L^{-1}, 1.15 mmol) and $FeCl_3$ solution (6.6 mL, 0.25 mol L^{-1}, 1.65 mmol) was well mixed at room temperature. The molar ratio of Fe^{3+}, Fe^{2+} and **CDPA/n4** in the above system was 100: 70: 15. To the reaction mixture was added aqueous ammonia (0.6 mL, 14.5 mol L^{-1}) to pH = 6–7, stirred for 15 min and then the pH = 8–9 was adjusted by using aqueous ammonia (about 0.2 mL). After aged at 80 °C for 30 min, black powder of **Fe_3O_4/CDPA/n4/0.52** (0.36 g) with 0.52 mmol g^{-1} loading capacity of **CDPA** was washed with deionized water (2 mL × 3) and dried under vacuum. The other MNPs-supported organocatalysts **Fe_3O_4/CDPA/n4/0.38** (0.32 g) and **Fe_3O_4/CDPA /n4/0.18** (0.27 g) with 0.38 mmol g^{-1} and 0.27 mmol g^{-1}loading capacities of **CDPA** were also prepared according to the same procedure, respectively at the molar ratios of Fe^{3+}, Fe^{2+}, **CDPA/ n4** = 100:70:10 and 100: 70:5.

General procedure for MNPs-supported organocatalysts by surface-modification method (Route 2)

The mixture of Fe_3O_4 MNPs (80–100 nm, 150.0 mg, 0.3 mmol), **CDPA/n4** (528.2 mg, 1.0 mmol) and methanol (10 mL) was stirred at 50 °C for 48 h, separated magnetically, washed with methanol (5 mL × 3) and dried overnight under vacuum at 50 °C to yield **Fe_3O_4@CDPA/n4** (0.28 g). According to the same procedure mentioned above, **CDPA/n2** and **CDPA/n6** instead of **CDPA/n4** were used to modify the surface of Fe_3O_4 MNPs to afford **Fe_3O_4 @CDPA/n2** (0.27g) and **Fe_3O_4@CDPA/n6/** (0.27g).

The determination of loading capacity of organocatalyst

Accurately weighed **Fe_3O_4/CDPA/n4/0.52** (m_1 = 29.0 mg) was dissolved in concentrated hydrochloric acid (38%, 1.5 mL) and neutralized by NaOH aqueous solution (12 mol L^{-1}) to pH = 12–13. The resulting precipitates (ferrous hydroxide and ferric hydroxide) were filtered and washed with deionized water (2 mL × 2). To the filtrate was added accurately H_3PO_4 (85%, m_2 = 15.2 mg) and volumed to 10.0 mL. Then the phosphorus content in the sample was determined by the quantitative ^{31}P NMR upon adding 0.54 mL of the solution into NMR tube by a syringe. The loading capacity of chiral organocatalyst **CDPA/n4** was calculated to be 0.52 mmol g^{-1} according to the following formula, in which A_1, A_2 were the peak areas of **CDPA/n4** and H_3PO_4 in ^{31}P NMR spectra respectively (see ESI†).

$$\frac{0.85\,A_1 m_2}{98\,A_2\,m_1} \times 10^3$$

General asymmetric aldol reaction

In a 25 mL vial, **Fe_3O_4/CDPA/n4/0.52** (36.0 mg, 5.0 mol %) containing 0.019 mmol of organocatalyst, TfOH (9.0 mg, 0.06 mmol), deionized water (1.5 mL) and cyclohexanone (0.71 g, 7.2 mmol) were added in turn. After stirred at room temperature for 15 min, *p*-nitrobenzaldehyde (57.4 mg, 0.38 mmol) was added and allowed to react at 20 °C for 24 h. The reaction process was monitored by TLC. After completion of the reaction, **Fe_3O_4/CDPA/n4/0.52** was magnetically separated by an external magnet. The resulting reaction mixture was quenched upon adding saturated NH_4Cl solution (10 mL) and extracted with ethyl acetate (5 mL × 3). The combined organic phases were dried over anhydrous Na_2SO_4 and evaporated under reduced pressure to afford the crude product, which was purified by flash column chromatography eluted with petroleum ether/ethyl acetate (*v/v* = 10/1→2/1) to give pure aldol adduct. Using 2-(hydroxy(4-methoxyphenyl)methyl)cyclohexanone as an example, its *anti/syn* ratio was determined by ^1H NMR method in $CDCl_3$, in which the chemical shifts of *syn*- and *anti*-C*H*OH protons were at δ 5.32 ppm (d) with ^3J = 1.3 Hz and δ 4.74 ppm (d) with ^3J = 8.8 Hz, respectively. The enantiomeric excess (%ee) was determined on a HPLC with a 254 nm UV-vis detector using Daicel chiralpak Chiral OD/AD column, eluting with *n*-hexane/ isopropanol (95/5) with a flow rate 0.5 mL min^{-1} under 20 °C.

Results and discussion

Preparation of supported organocatalyst

Due to the high solubility product constant (pKsp) of phosphate, phosphonic acid (-PO_3H_2) can easily react with many metal ions such as Zr^{4+}, Ti^{4+}, Fe^{3+} and Fe^{2+} to afford the corresponding phosphonate precipitates.[14] In this study, MNPs-supported organocatalysts were prepared by surface-modification and co-precipitation methods, taking advantage of chemical reactivity of phosphonic acid (-PO_3H_2) with Fe^{3+} and Fe^{2+} ions. In the course of co-precipitation method (Route 1, **Fig.1**), Fe_3O_4 MNPs and iron (ferrous) phosphonate were simultaneously formed in the pH = 8–10 range upon adding aqueous ammonia to the mixture of organocatalyst **CDPA/n4**, aqueous $FeCl_2$ and $FeCl_3$ solution. Given that ferrous and iron phosphonates could share the same iron atom with Fe_3O_4 crystal lattice through the oxygen atom in phosphonate, organocatalyst **CDPA/n4** could firmly embed itself in the hybrid framework of Fe_3O_4 and ferrous and iron phosphonates by means of phosphonic acid (-PO_3H_2) as an anchor point. There were three particularly important points worthy of much attention. First of all, the loading capacities (0.18–0.52 mmol g^{-1}) of chiral organocatalyst **CDPA/n4**, determined by quantitative ^{31}P NMR, increased with the increase of used **CDPA/n4** during the synthetic procedure (**Table 1**). Secondly, organocatalyst **CDPA/n4** could be quantitatively anchored into the hybrid backbone, which was very important for expensive chiral compound from green chemistry. Finally, it was noteworthy that the pH value played an important role in the loading capacity of **CDPA/n4** during preparation process. When the medium pH was above 11, the loading capacity of **CDPA/n4** had a sharp drop owing to the chemical transformation of ferrous and iron phosphonate into Fe_3O_4. The optimal pH suitable for quantitative anchorage of organocatalyst was found to be in the 8-10 range. Overall, the co-precipitation method could readily achieve the tunable and high loading capacities of organocatalysts at room temperature through direct one-pot synthesis.

For comparison, surface-modification provided an alternative method to yield MNPs-supported organocatalyst in direct synthesis strategy by means of the chemical reaction of phosphonic acid as an anchor point with Fe_3O_4 in CH_3OH medium at 50 °C (route 2, **Fig.1**). However, due to the difficult insertion of phosphonic acids into the preformed Fe_3O_4 crystal lattices on the surface or internal pores, the maximal loading capacities of organocatalysts were significantly reduced to the 0.20-0.23 mmol g^{-1} ranges, even at the higher used amount of organocatalyst and more prolonged

reaction time (72 h at 50 °C) (Table 1).

Table 1 The loading capacities of organocatalysts

Supported Cat.	Weight (g)	Used Cat. (mg)	Loading capacity (mmol g^{-1})
Fe_3O_4/CDPA/n4/0.52[a]	0.36	130.0	0.52
Fe_3O_4/CDPA/n4/0.38[a]	0.32	86.7	0.38
Fe_3O_4/CDPA/n4/0.18[a]	0.27	43.3	0.18
Fe_3O_4@CDPA/n2[b]	0.27	528.2	0.22
Fe_3O_4@CDPA/n4[b]	0.28	559.2	0.24
Fe_3O_4@CDPA/n6[b]	0.27	589.0	0.20

[a] co-precipitation method: 1.15 mmol $FeCl_2$, 1.66 mmol $FeCl_3$ at room temperature in pH=8-10 range. [b] Surface-modification: 1.0 mmol CDPA and 150 mg Fe_3O_4 MNPs in CH_3OH for 48 h at 50 °C.

Characterization of supported organocatalysts

TEM and HRTEM. The TEM images were used to obtain the information on the particle sizes and morphologies of **Fe_3O_4/CDPA** and **Fe_3O_4@CDPA**, respectively prepared by co-precipitation and surface-modification methods.

The typical TEM images of **Fe_3O_4@CDPA/n4** were shown in Fig. 2. Compared with the bare Fe_3O_4, the similar square particles of **Fe_3O_4@CDPA/n4** with the diameters of *ca.* 80-100 nm and electron diffraction pattern (inset of Fig.2-a, b) were observed, which illustrated that there was no great change in the skeleton structure of Fe_3O_4 after surface-modification. Furthermore, from Fig.2-d, it was found that the preformed Fe_3O_4 MNPs were covalently coated with a discontinuous and thin layers of chiral organocatalyst **CDPA/n4** by means of phosphonic acid (-PO_3H_2) anchor points. Especially, our endeavours to elucidate the chemical reaction of phosphonic acid with Fe^{3+} and Fe^{2+} ions on the surface of Fe_3O_4 were also supported by the selected HRTEM images shown in Fig.2-f, in which the highly ordered arrays of Fe_3O_4 crystal were etched by phosphonic acid (-PO_3H_2) and became blurred (Fig.2-e).

Fig.2 The TEM and HRTEM images of Fe_3O_4 MNPs (a, c, e) and **Fe_3O_4@CDPA/n4** (b, d, f).

Fig. 3 The TEM and HRTEM images of **Fe_3O_4/CDPA/n4/0.52**

From Fig.3, the different structural features and spherical morphologies of MNPs-supported organocatalysts **Fe_3O_4/CDPA/n4** were achieved by co-precipitation method. Using **Fe_3O_4/CDPA/n4/0.52** as an example, its electron diffraction pattern (inset of Fig.3) exhibited the non-crystalline and long range-disordered nature of the material with the non-uniform diameters of 10-20 nm. However, the short range-ordered crystalline structure with the interplanar lattice spacing (0.22 nm) for Fe_3O_4 (311) was evidenced from the HRTEM images and also supported by X-ray diffraction measurements (**Fig.4**). It was noteworthy that the larger crystallographic planes of **Fe_3O_4/CDPA/n4/0.52** than Fe_3O_4 were arranged in the crisscross and intermittent patterns owing to the embedded **CDPA/n4** organocatalyst by anchor point (-PO_3H_2).

Fig. 4 Powder X-ray diffraction patterns of Fe_3O_4 (a), **Fe_3O_4@CDPA/n4** (b), **Fe_3O_4/CDPA/n4/0.18** (c) and **Fe_3O_4CDPA/n4/0.52** (d)

XRD. Fig. 4 displayed the high-angle powder XRD patterns of Fe_3O_4 and various MPNs-supported organocatalysts. From Fig. 4-a, the XRD pattern of bare Fe_3O_4 had the typical peaks at 18.12°, 30.08°, 35.45°, 43.06°,53.49°, 57.00°, 62.62° and 74.05°, which corresponded to the {111, d = 5.68 Å}, {220, d = 3.44 Å}, {311, d = 2.94 Å}, {400, d = 2.44 Å}, {422, d = 1.99 Å}, {511, d = 1.87 Å}, {440, d = 1.72 Å} and {533, d = 1.48 Å} reflections, respectively. The interplanar spacings of 3.44 Å and 5.68 Å for the {220} and {111} planes were consistent with the bulk values of Fe_3O_4 with the inverse spinel structure.[15] These characteristic reflections of Fe_3O_4 were also present in the powder XRD patterns of **Fe_3O_4@CDPA/n4** (Fig. 4-b), suggesting that the modification of **CDPA/n4** on the surface Fe_3O_4 MNPs did not significantly affect the phase composition of Fe_3O_4. Moreover, **Fe_3O_4/CDPA/n4/0.18** with the low loading capacity of **CDPA/n4** (0.18 mmol g^{-1}) showed the broad and characteristic XRD peaks (220, 311, 400, 511, 440) with the low relative intensities, which also matched well with those of magnetite and elucidated the similar inverse spinel structure as magnetite. However, with the increase of the loading capacities of **CDPA/n4** from 0.18 mmol g^{-1} to 0.52 mmol g^{-1}, some characteristic XRD peaks of **Fe_3O_4/CDPA/n4/0.52** (220, 400 and 511) disappeared and all of the relative intensities were weakened sharply. It was demonstrated that the noncrystalline nature of **Fe_3O_4/CDPA/n4/0.52** was strengthened due to the attachment of **CDPA/n4** by co-precipitation, just as its electron diffraction pattern exhibited (inset of Fig.3).

Fig. 5 Thermogravimetric curves of **Fe_3O_4@CDPA/n 4** (a), **Fe_3O_4/CDPA/n4/0.18** (b), **Fe_3O_4/CDPA/n4/0.38** (c), and **Fe_3O_4/CDPA/n4 /0.52** (d)

TGA analysis. Thermal analysis was performed to monitor the decomposition profiles for **Fe_3O_4/CDPA/n4** and **Fe_3O_4@CDPA /n4**, and their results were depicted in Fig. 5. The weight losses of both **Fe_3O_4/CDPA/n4** and **Fe_3O_4@CDPA/n4** below 200 ºC were assigned to the release of physisorbed and chemisorbed waters in the internal and external surface. The weight losses in the temperature range of 200–800 ºC in the TGA curves were attributed to the decomposition of the grafted **CDPA/n4**. Meanwhile, the total weight losses in the 200–800 ºC range were found to be 11.63, 9.26, 18.95 and 24.77 %, respectively for **Fe_3O_4@CDPA/n4** and **Fe_3O_4/CDPA/n4** with the different loading capacities (0.18, 0.38 and 0.52 mmol g^{-1}). Based on these weight losses, the loading **CDPA/n4** contents were calculated to be 0.22, 0.18, 0.40 and 0.51 mmol g^{-1}, which were very close to the results determined by ^{31}P NMR (Table 1).

Porous structure. The BET-specific surface areas, average pore diameters and pore volumes for as-synthesized catalysts were listed in Table 2, and their nitrogen adsorption-desorption isotherm plots, performed at 77 K, were shown in ESI†.

Fig. 6 The pore size distributions (PSDs) of **Fe_3O_4@CDPA/n4** (a), **Fe_3O_4/CDPA/n4/0.18** (b), **Fe_3O_4/CDPA/n4/0.38** (c), and **Fe_3O_4/CDPA /n4/0.52** (d).

The N_2 adsorption-desorption isotherms of **Fe_3O_4** and **Fe_3O_4@CDPA/n4** accorded with Type II isotherm in classic definitions, which matched well the normal form obtained with a non-porous or macroporous adsorbent, whereas **Fe_3O_4/CDPA/n4** showed Type IV isotherm associated with capillary condensation like

industrial mesoporous adsorbents (see ESI†).[16] From **Table 2**, it was found that the surface modification did not affect significantly the performed porous structure of Fe_3O_4. However, the lower BET-specific surface area (6.83 m^2 g^{-1}) and pore volume (18.1 × 10^{-3} cc g^{-1}) of **Fe_3O_4@CDPA/n4** than bare Fe_3O_4 were observed. Interestingly, the BET-specific surface areas and pore volumes of various **Fe_3O_4/CDPA/n4** by co-precipitation increased remarkably due to the supporting effect of **CDPA/n4** organocatalyst. The pore size distributions (PSDs) of **Fe_3O_4/CDPA/n4** suggested the existence of 2-25 nm regular mesopores (**Fig. 6**). Especially, the more **CDPA/n4** (0.18 → 0.52 mmol g^{-1}) were loaded into the backbone of Fe_3O_4, the larger average pore diameters (9.8 → 15.0 nm) and higher pore volumes (0.11 → 0.15 cc g^{-1}) were achieved. Regretfully, the lower BET-specific surface areas were resulted from the blockage of appended **CDPA/n4** in the inner mesopores.

Table 2 The surface areas, average pore diameters and pore volumes of MNPs-supported organocatalysts[a]

Cat.	Surface area m^2 g^{-1} [b]	Average pore diameter [Å] [c]	Pore Volume [cc g^{-1}] [c]
Fe_3O_4	7.91	103.8	20.5
Fe_3O_4@CDPA/n4	6.83	105.8	18.1
Fe_3O_4/CDPA/n4/0.18	82.8	98.0	111.7
Fe_3O_4/CDPA/n4/0.38	50.7	109.1	125.8
Fe_3O_4/CDPA/n4/0.52	40.2	150.4	151.3

[a] The samples were degassed at 105 °C for 5 h. [b] Based on the multipoint BET method. [c] Based on the desorption data using BJH method.

Magnetic property. The magnetic properties of MNPs-supported organocatalysts were examined through vibrating sample magnetometry (VSM). The hysteresis loops at room temperature were shown in **Fig. 7**.

Fig. 7 The magnetization curves of Fe_3O_4, **Fe_3O_4@CDPA/n4** (a), **Fe_3O_4/CDPA/n4/0.18** (b), **Fe_3O_4/CDPA/n4/0.38** (c), and **Fe_3O_4/CDPA/n4/0.52** (d).

From **Fig.7**, the same saturation magnetization value for **Fe_3O_4@CDPA/n(4)** and bare **Fe_3O_4** was found to be 53.36 emu g^{-1}, which elucidated that the magnetic property was not influenced by the surface modification method. However, the saturation magnetizations of **Fe_3O_4/CDPA/n4**, prepared by co-precipitation, decreased with the increase of loaded **CDPA/n4** organocatalysts. VSM analysis showed that **Fe_3O_4/CDPA/n4** catalysts possessed the saturated magnetization values of 44.06, 11.75 and 10.65 emu g^{-1}, respectively at the 0.18, 0.38 and 0.52 mmol g^{-1} loading capacities. These values were all sufficient enough to meet the need of magnetic separation.[17, 11] The zero coercivity and resonance of each magnetization loop evidenced the superparamagnetism behavior at 298 K for all the samples, which was very useful for the catalyst's rapid dispersion and separation.

From the above characterization methods, it was concluded that MNPs-supported organocatalysts **Fe_3O_4/CDPA/n4** by co-precipitaion exhibited the higher loading capacities, BET-specific surfaces, average pore diameters and pore volumes than **Fe_3O_4@CDPA/n4** by surface-modification, which were beneficial to perfect catalytic activity.

Catalytic performance

With two novel types of MNPs-supported organocatalysts in hand, prepared by co-precipitation and surface-modification methods, their catalytic performances including activity and steroselectivity were evaluated in the well-documented aldol reaction between 4-nitrobenzaldehyde and cyclohexanone.[18]

Table 3 The asymmetric aldol reaction of *p*-nitrobenzaldehyde and cyclohexanone catalyzed by various MNPs-supported organocatalysts [a]

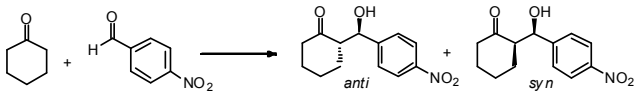

Entry	Cat.	Time (h)	Yield (%)[b]	Dr (*anti/syn*)[c]	*Anti* (%ee) [d]
1	Fe_3O_4@CDPA/n2	48	92	82:18	93
2	Fe_3O_4@CDPA/n4	48	98	86:14	96
3	Fe_3O_4@CDPA/n6	48	88	77:23	86
4	Fe_3O_4/CDPA/n4/0.18	48	>99	89:11	96
5	Fe_3O_4/CDPA/n4/0.38	24	>99	89:11	96
6	Fe_3O_4/CDPA/n4/0.52	12	>99	90:10	98
7	Fe_3O_4/CDPA/n2/0.19	12	>99	90:10	96
8	Fe_3O_4/CDPA/n6/0.19	12	>99	88:12	95
9	CDPA/n2[e]	48	90	89:11	94
10	CDPA/n4[e]	48	92	84:16	95
11	CDPA/n6[e]	48	88	86:14	93

[a] Reaction conditions: 20 ºC, *p*-nitrobenzaldehyde (56.0 mg, 0.37 mmol), cyclohexanone (0.7 g, 7.1 mmol), 5.0 mol% cat., 1.5 mL of water, TfOH (9.0 mg, 0.06 mmol). [b] Isolated yield. [c] Determined by ^{1}H NMR. [d] Monitored by chrial HPLC with Daicel Chiralpak OD-H column. [e] "blank" aldol reactions.

Under optimum catalytic conditions, the comparative tests of various MNPs-supported organocatalysts were performed and the catalytic results were summarized in **Table 3**. Although the various **Fe_3O_4@CDPA/n** with the different arm chain lengths (n = 2, 4 and 6) had the similar loading capacities in the 0.20–0.23 mmol g^{-1} range (**Table 1**), the arm chain lengths played an important role in the yields and steroselectivities of aldol adduct. The optimum arm chain length was found to be n = 4 in terms of enantioselectivity, diastereoselectivity and reactivity (98%, *anti/syn* = 86/14, 96 %ee *anti*) (**entry 2**). Meanwhile, compared with **Fe_3O_4@CDPA/n4** (48 h, 88–98% yield, *anti/syn* = 77–84/23–16, 86–96 %ee *anti*, **entries 1–3**) and "blank" **CDPA/n** (48 h, 87–95% yield, *anti/syn* = 86–89/14–11, 93–94 %ee *anti*, **entries 9–11**), **Fe_3O_4/CDPA/n(4)**, prepared by co-precipitation method, afforded the better catalytic performances (>99%, *anti /syn* = 90/10, 96–98 %ee *anti*, **entries 4–6**). Among them, **Fe_3O_4/CDPA/n4/0.52** with the highest loaded organocatalyst (0.52 mmol g^{-1}) produced the most excellent catalytic performances (12 h, >99%, *anti/syn* = 90/10, 98 %ee *anti*, **entry 6**). These enhanced catalytic results were related to the improved mass transfer originating from the nano size, regular mesopores and higher pore volume mentioned above (**Table 2** and **Fig.6**). Unfortunately, **Fe_3O_4/CDPA/n4** afforded the less catalytic activities at the lower loading capacities of **CDPA/n4** (48 h at 0.18 mmol g^{-1}; 24 h at 0.38 mmol g^{-1}), although excellent diastereoselectivity and enantioselectivity were maintained at the same level (**entries 4, 5**).

Table 4 The asymmetric aldol reaction of benzaldehyde derivatives with cyclohexanone catalyzed by **Fe_3O_4@CDPA/n4** [a]

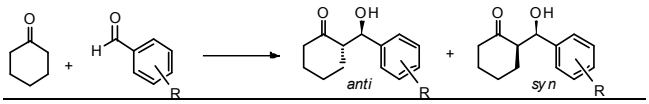

Entry	R	Time (h)	Yield (%)[b]	Dr (*anti/syn*)[c]	*Anti*-adduct (%ee) [d]
1	2-NO_2	24	60	90:10	97
2	3-NO_2	24	90	86:14	92
3	4-NO_2	24	94	84:16	95
4	3-CN	24	64	91:9	95
5	4-CN	24	94	83:17	95
6	4-Cl	48	63	79:21	89
7	4-Br	48	44	79:21	90
8	4-CH_3	96	-		
9	4-OCH_3	96	-		

[a] Reaction conditions: 20 ºC, **Fe_3O_4@CDPA/n4**, *p*-nitrobenzaldehyde (56.0 mg, 0.37 mmol), cyclohexanone (0.7 g, 7.1 mmol), 5 mol% cat., 1.5 mL of water, TfOH (9.0 mg, 0.06 mmol). [b]Isolated yield. [c] Determined by ^{1}H NMR. [d] Monitored by HPLC with Daicel Chiralpak AD/OD-H column.

Although **Fe_3O_4@CDPA/n4** had the good catalytic performance in the aqueous aldol reaction between cyclohexanone and various benzaldehydes bearing strong electron-withdrawing groups such as –NO_2 and -CN groups (**Table 4, entries 1-5**), the unsatisfactory results with the lower diastereoselectivity (*anti/syn* = 79/21) and less yields (44–63%) were obtained for the halogenated benzaldehydes with weak electron-withdrawing groups (**entries 6, 7**). Regrettably, the aromatic aldehydes with electron-donating groups such as –CH_3 and –OCH_3 groups did not undergo the aldol reaction smoothly due to the low 0.20–0.23 mmol g^{-1} loading capacities of **CDPA/n4** organocatalyst (**entries 8, 9**).

Delightedly, excellent performances of **Fe_3O_4/CDPA/n4/0.52** were observed in the direct asymmetric aldol reaction of cyclohexanone with various aromatic aldehydes using water as a solvent (**Table 5, entries 1-14**). In all cases, the aromatic aldehydes with electron-withdrawing groups including –NO_2, X and -CN afforded the aldol adducts in the good to high yields (>86 %) and steroselectivities (*anti/syn* = 82–98/18–2 and 93–98 %ee *anti*, **entries 1-8**). Meanwhile, the aromatic aldehydes with strong electron-donating substituents (–CH_3 and –OCH_3) produced the corresponding *β*-hydroxy ketone in the moderate to good yields (36–97%) and steroselectivities (*anti/syn* = 82–96/18–4 and 75–97 %ee *anti*, **entries 9-14**). Although the steric hindrance resulted in the less catalytic activity, the 2-substituted benzaldehydes, both with electron-withdrawing and electron-donating substituents, gave the better steroselectivities owing to the positive enantioface discrimination in the transition state (**entries 1, 6, 9** and **12**). Furthermore, compared with the homogeneous **CDPA/n4**. **Fe_3O_4/CDPA/n4/0.52** exhibited the higher yields and steroselectivities for most substituted benzaldehydes (entries 1–14),

Table 5 The asymmetric aldol reaction of benzaldehyde derivatives with cyclohexanone [a]

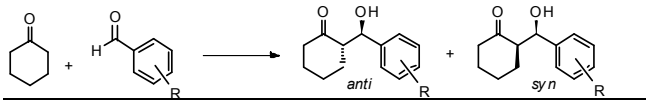

Entry	R	Time (h)	Yield (%)[b]	*anti/syn* [c]	%ee *anti* [d]
1	2-NO_2	24	>99	94:6	96
	2-NO_2[e]	48	89	95:5	97
2	3-NO_2	24	>99	90:10	98
	3-NO_2[e]	48	98	90:10	98
3	4-NO_2	8	>99	90:10	97
	4-NO_2[e]	24	97	89:11	97
4	3-CN	24	95	86:14	97
	3-CN [e]	48	89	85:15	97
5	4-CN	24	92	82:18	96
	4-CN[e]	48	82	84:16	97
6	2-Cl	48	87	98:2	96
	2-Cl[e]	48	76	95:5	94
7	3-Cl	48	90	96:4	95
	3-Cl[e]	48	80	95:5	95
8	4-Cl	48	97	94:6	93
	4-Cl[e]	48	79	95:5	98
9	2-CH_3	48	87	90:10	97
	2-CH_3[e]	96	80	89:11	95
10	3-CH_3	48	91	90:10	89
	3-CH_3[e]	96	85	90:10	97
11	4-CH_3	48	97	94:6	79
	4-CH_3[e]	96	80	95:5	82
12	2-OCH_3	48	36	96:4	92
	2-OCH_3[e]	96	40	95:5	90
13	3-OCH_3	48	51	82:18	91
	3-OCH_3[e]	96	59	84:16	92
14	4-OCH_3	48	57	88:12	75
	4-OCH_3[e]	96	43	86:14	83
15	2-NO_2	24	76	86:14	-94
16	3-NO_2	24	95	81:19	-93
17	4-NO_2	12	>99	77:23	-91
18	3-CN	24	87	80:20	-92
19	4-CN	24	99	77:23	-89
20	2-Cl	48	94	89:11	-94
21	3-Cl	48	89	70:30	-78
22	4-Cl	48	96	79:21	-93
23	2-CH_3	48	37	88:12	-93
24	3-CH_3	48	43	91:9	-91
25	4-CH_3	48	48	94:6	-93
26	2-OCH_3	48	16	81:19	-84
27	3-OCH_3	48	31	83:17	-93
28	4-OCH_3	48	21	79:21	-87

[a] Reaction conditions: 20 ºC, 5 mol% Cat.: **Fe_3O_4/CDPA/n4/0.52** (entries 1-14) or **Fe_3O_4/CNPA/n4** (entries 15-28), *p*-nitrobenzaldehyde (56.0 mg, 0.37 mmol), cyclohexanone (0.7 g, 7.1 mmol), 1.5 mL of water, TfOH (9.0 mg, 0.06 mmol). [b] Isolated yield. [c] Determined by ^{1}H NMR. [d] Monitored by chrial HPLC, Daicel Chiralpak AD-H or OD-H column. [e] homogeneous organocatalyst **CDPA/n4**.

When organocatalyst **CNPA/n4** with (8R, 9R) configuration was used as a catalyst instead of **CDPA/n4** with (8S, 9S) configuration, the corresponding MNPs-supported organocatalyst **Fe_3O_4/CNPA/n4/0.49** with 0.49 mmol g^{-1} loading capacity was also prepared by co-precipitation method. As expected, **Fe_3O_4/CNPA/n4/0.49** smoothly catalyzed the aldol additions to afford the opposite enantiomers (R = -NO_2, X, CN CH_3 and OCH_3) in the good catalytic performances (21–99% yield, *anti/syn* = 70–94/30–6 and -78–-94 %ee *anti*, **Table 5, entries 15–28**). However, the catalytic performances of **Fe_3O_4/CNPA/n4/0.49** including activities and

steroselectivities were slightly inferior to that of **Fe_3O_4/CDPA/n4 /0.52**, possibly resulted from the inferior mutual matching pattern of (8R, 9R) configuration of **CNPA/n4** with the reactants.

In conclusion, based on the catalytic results in aldol reaction, the novel **Fe_3O_4/CDPA/n4**, prepared by one-pot co-precipitation, acted as an efficient supported organocatalyst in aqueous asymmetric aldol reaction and gave the better catalytic performances than **Fe_3O_4@CDPA/n4** through surface-modification method.

The recovery and reuse of supported organocatalyst

Apart from excellent catalytic efficiency in aqueous aldol reaction, another important feature of **Fe_3O_4/CDPA/n4/0.52** was its easy and quantitative recovery from the reaction mixture by using an external magnet.

Table 6 Recycling experiment of **Fe_3O_4/CDPA/n4/0.52** in the aldol reaction between 4-nitrobenzaldehyde and cyclohexanone [a]

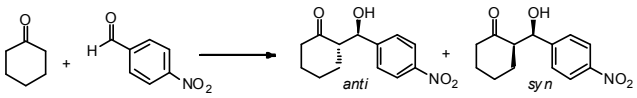

Entry	Run times	Time (h)	Yield (%)[b]	Dr (*anti/syn*)[c]	*Anti*-adduct (%ee) [d]
1	1	12	>99	90:10	98
2	2	24	>99	89:11	98
3	3	24	98	87:13	96
4	4	24	95	88:12	97
5	5	24	95	88:12	95
6	6	48	93	89:11	96
7	7	48	90	77:23	92

[a] Reaction conditions: 20 ºC, 5.0 mol% **Fe_3O_4/CDPA/n4/0.52**, *p*-nitrobenzaldehyde (56.0 mg, 0.37 mmol), cyclohexanone (0.7 g, 7.1 mmol), 1.5 mL of water, TfOH (9.0 mg, 0.06 mmol). [b] Isolated yield. [c] Determined by ^{1}H NMR. [d] Monitored by chrial HPLC with Daicel Chiralpak OD-H column.

Fig. 8 The pore size distributions (PSDs) and TEM images of the fresh (a, c) and 7th-recovered **Fe_3O_4/CDPA/n4/0.52** (b, d)**,**

Table 6 showed the results of the recovery and reusability of **Fe_3O_4/CDPA/n4/0.52** in the asymmetric aldol reaction of cyclohexanone with 4-nitrobenzaldehyde in water. From Table 6, **Fe_3O_4/CDPA/n4/0.52** could be easily recycled and reused for up to six times with no appreciable decrease in the yields and steroselectivities of aldol product, which demonstrated that **Fe_3O_4/ CDPA/n4/0.52** possessed good stability and reusability. However, it was found that there was a sharp drop in the steroselectivity (*anti/syn* = 89/11→77/23 and 96→92 %*anti*) in the seventh time. In order to seek the reason why catalytic performances decreased, nitrogen adsorption-desorption isotherm, TEM, TGA and ^{31}P NMR were used to monitor the surface morphology, weight loss percent of organic moiety and pore structure of the 7th -recycled **Fe_3O_4/CDPA/n4/0.52**. By means of ^{31}P NMR, **Fe_3O_4/CDPA/n4 /0.52** did not have an obvious change in the loading capacity of **CDPA/n4** (0.50 mmol g^{-1}) after reused for seven times. However, compared with the fresh **Fe_3O_4/ CDPA/n4/0.52**, the agglomeration of particles was observed from the TEM images (Fig.8-d). Furthermore, the organic weight loss of recovered **Fe_3O_4/CDPA/ n4/0.52** in the temperature range of 150–800 °C increased from 22.8 to 28.5%, and the average pore diameter, BET-specific surface area and pore volume decreased from 150.4 Å, 40.2 m^2 g^{-1} and 0.151 cc g^{-1} to 14.6 Å, 37.0 m^2 g^{-1}, 0.014 cc g^{-1}, respectively. From Fig.8-b, the pore size distributions (PSDs) suggested that some mesopores in the 2-25 nm range were occupied and disappeared. It was speculated that the adsorbed reactants, products, or impurities occupied those regular mesopores, covered catalytic active sites, and resulted in the decrease in catalytic performance.

Conclusions

A novel type of efficient and magnetically recoverable Fe_3O_4 MNPs-supported organocatalysts was successfully prepared by facile one-pot co-precipitation and surface-modification methods, taking advantage of phosphonic acid (-PO_3H_2) as an anchor point. Compared with surface-modification method, the co-precipitation method could quantitatively and easily afford MNPs-supported organocatalysts with controllable loading capacity of organocatalyst and higher BET-specific surface area, average pore diameter and pore volume. These MNPs-supported organocatalysts, prepared by facile one-pot co-precipitation, not only possessed excellent catalytic performance in asymmetric aldol reaction, but also could be well dispersed in the aqueous reaction medium and easily magnetically recovered by using an external magnet. Furthermore, there was no significant loss of catalytic performance in asymmetric aldol reaction, even in the sixth time in water.

Acknowledgments

The work was supported by the National Science Foundation of China (grants. 21071116).

Notes and references

College of Chemistry and Chemical Engineering, Southwest University, Chongqing, 400715, P. R. China . Fax: (+86)23-68253237; Tel: (+86)23-68253237; E-mail: zcj123@swu.edu.cn

† Electronic Supplementary Information (ESI) available: ^{1}H, ^{13}C and ^{13}P NMR and MS spectra of **CDPE**, **CDPA**, **CNPE** and **CNPA**, TGA, N_2 adsorption-desorption isotherm and HPLC and ^{1}H NMR of aldol products. See DOI: 10.1039/b000000x/

1 (a) V. Polshettiwar, R. Luque, A. Fihri, H. B. Zhu, M. Bouhrara and J. M. Basset, *Chem. Rev.*, 2011, **111**, 3036–3075; (b) D. H. Zhang, C. Zhou, Z. H. Sun, L. Z. Wu, C. H. Tung and T. R. Zhang, *Nanoscale*, 2012, **4**, 6244–6255; (c) R. B. N. Baig and R. S. Varma, *Chem. Commun.*, 2013, **49**, 752–770; (d) M. B. Gawande, P. S. Brancoa and R. S. Varma, *Chem. Soc. Rev.*, 2013, **42**, 3371–3393; (e) R. Ricco, L. Malfatti, M. Takahashi, A. J. Hill and P. Falcaro, *J. Mater. Chem. A*, 2013, **1**, 13033–13045; (f) S. Behrens, *Nanoscale*, 2011, **3**, 877–892.

2 M. K. Schröter, L. Khodeir, M. W. E. van den Berg, T. Hikov, M. Cokoja, S. Miao, W. Grünert, M. Muhler and R. A. Fischer, *Chem. Commun.*, 2006, 2498–2500.

3 (a) I. Lee, Q. Zhang, J. Ge, Y. Yin and F. Zaera, *Nano Res.*, 2010, **4**, 115–123; (b) I. Lee, M. A. Albiter, Q. Zhang, J. Ge, Y. Yin and F. Zaera, *Phys. Chem. Chem. Phys.*, 2011, **13**, 2449–2456; (c) Y. Deng, Y. Cai, Z. Sun, J. Liu, C. Liu, J. Wei, W. Li, C. Liu, Y. Wang and D. Zhao, *J. Am. Chem. Soc.*, 2010, **132**, 8466–8473; (d) S. S. Lee, S. N. Riduan, N. Erathodiyil, J. Lim, J. L. Cheong, J. Cha, Y. Han and J. Y. Ying, *Chem.–Eur. J.*, 2012, **18**, 7394–7403.

4 (a) S. C. Tsang, V. Caps, I. Paraskevas, D. Chadwick and D. Thompsett, *Angew. Chem., Int. Ed.*, 2004, **43**, 5645–5649; (b) H. Yoon, S. Ko and J. Jang, *Chem. Commun.*, 2007, 1468–1470; (c) W. Teunissen, F. M. F de Groot, J. Geus, O. Stephan, M. Tence and C. Colliexy, *J. Catal.*, 2001, **204**, 169–174; (d) L. Hu, S. Dang, X. Yang and J. Dai, *Microporous Mesoporous Mater.*, 2012, **147**, 188–193; (e) M. Zhu and G. Diao, *J. Phys. Chem. C*, 2011, **115**, 24743–

24749; (f) S. Wu, Q. He, C. Zhou, X. Qi, X. Huang, Z. Yin, Y. Yang and H. Zhang, *Nanoscale*, 2012, **4**, 2478–2483.

5 (a) S. Xuan, W. Jiang, X. Gong, Y. Hu and Z. Chen, *J. Phys. Chem. C*, 2009, **113**, 553–558; (b) S. Ko and J. Jang, *Angew. Chem., Int. Ed.*, 2006, **45**, 7564–7567; (c) B. Liu, W. Zhang, F. Yang, H. Feng and X. Yang, *J. Phys. Chem. C*, 2011, **115**, 15875–15884; (d) C. Jang, M. Chen, S. Xuan, W. Jang, X. Gong and Z. Zhang, Can. J. Chem., 2009, **87**, 502–506; (e) B. Dong, D. L. Miller and C. Y. Li, *J. Phys. Chem. Lett.*, 2012, 1346–1350.

6 (a) B. Baruwati, D. Guin and S. V. Manorama, *Org. Lett.*, 2007, **9**, 5377–5380; (b) V. Polshettiwar, B. Baruwati and R. S. Varma, *Green Chem.*, 2009, **11**, 127–131; (c) V. Polshettiwar and R. S. Varma, *Chem.–Eur. J.*, 2009, 15, 1582–1586; (d) R. Abu-Reziq, D. Wang, M. Post and H. Alper, *Adv. Synth. Catal.*, 2007, **349**, 2145–2150; (e) Y. Wang and J.-K. Lee, *J. Mol. Catal. A: Chem.*, 2007, **263**, 163–168; (f) Y. Zhu, C. P. Ship, A. Emi, Z. Su, Monalisa and R. A. Kemp, *Adv. Synth. Catal.*, 2007, **349**, 1917–1922; (g) L. M. Rossi, L. L. R. Vono, F. P. Silva, P. K. Kiyohara, E. L. Duarte and J. R. Matos, *Appl. Catal., A*, 2007, **330**, 139–144; (h) D. Guin, B. Baruwati and S. V. Manorama, *Org. Lett.*, 2007, **9**, 1419–1421.

7 (a) K. Azizi and A. Heydari, *RSC Adv.*, 2014, **4**, 6508–6512; (b) M. B. Gawande, A. Velhinho, I. D. Nogueira, C. A. A. Ghumman, O. M. N. D. Teodorod and P. S. Branco, *RSC Adv.*, 2012, **2**, 6144–6149.

8 (a) A. G. Doyle and E. N. Jacobsen, *Chem. Rev.*, 2007, **107**, 5713–5743; (b) P. Melchiorre, M. Marigo, A. Carlone and G. Bartoli, *Angew. Chem. Int. Ed.*, 2008, **47**, 6138–6171; (c) A. Dondoni and A. Massi, *Angew. Chem. Int. Ed.*, 2008, **47**, 4638–4660; (d) M. D. D. de Villegas, J. A. Gálvez, P. Etayo, R. Badorrey and P. López-Ram-de-Víu, *Chem. Soc. Rev.*, 2011, **40**, 5564–5587; (e) L. Jiang and Y. C. Chen, *Catal. Sci. Technol.*, 2011, **1**, 354–365; (f) C. H. Cheon and H. Yamamoto, *Chem. Commun.*, 2011, **47**, 3043–3056; (g) J. Mlynarski and B. Gut, *Chem. Soc. Rev.*, 2012, **41**, 587–596; (h) J. F.Briére, S. Oudeyer, V. Dalla and V. Levacher, *Chem. Soc. Rev.*, 2012, **41**, 1696–1707; (i) D. Bonne, T. Constantieux, Y. Coquerel and J. Rodriguez, *Org. Biomol. Chem.*, 2012, **10**, 3969–3973.

9 (a) M. Gruttadauria, F. Giacalone and R. Noto, *Chem. Soc. Rev.*, 2008, **37**, 1666–1688; (b) L. W. Xu, L. Li and Z. H. Shi, *Adv. Synth. Catal.*, 2010, **352**, 243–279; (c) A. M. Caminade, A. Ouali, M. Keller and J. P. Majoral, *Chem. Soc. Rev.*, 2012, **41**, 4113–4125; (d) F. Cozzi, *Adv. Synth. Catal.*, 2006, **348**, 1367–1390.

10 S. Luo, X. Zheng and J. Cheng, *Chem. Commun.*, 2008, 5719–5721.

11 H. Yang, S. Li, X. Wang, F. Zhang, X. Zhong, Z. Dong and J. Ma, *J. Mol. Catal. A: Chem.*, 2012, **363–364**, 404–410.

12 Y. Kong, R. Tan, L. L. Zhao and D. H. Yin, *Green Chem.*, 2013, **15**, 2422–2433.

13 (a) W. Wang, X. Ma, J. Wan, J. Cao and Q. Tang, *Dalton Trans.*, 2012, **41**, 5715–5726; (b) J. Wan, X. Ma, R. He and M. Li, *Chin. Chem. Lett.*, 2014, **25**, 557–560.

14 (a) J. Mi, C. Wang, N. Chen, R. Li and Y. Pan, *J. Solid State Chem.*, 2010, **183**, 2763–2769; (b) Y. Zhang, Y. Qi, Y. Zhang, Z. Liu,Y. Zhao and Z. Liu, *Mater. Res. Bull.*, 2007, **42**, 1531–1538

15 (a) M. Z. Kassaee, H. Masrouri and F. Movahedi, *Appl. Catal., A*, 2011, **395**, 28–33; (b) M. V. Kovalenko, M. I. Bodnarchuk, R. T. Lechner, G. Hesser, F. Schaffler and W. Heiss, *J. Am. Chem. Soc.*, 2007, **129**, 6352–6353.

16 K. S. W. Sing, D. H. Everett, R. A. W. Haul, L. Moscou, R. A. Pierotti, J. Rouquerol and T. Siemieniewska, *Pure Appl. Chem.*, 1985, **57**, 603–619.

17 W. Wang, Y. Xu, D. I. C. Wang and Z. Li, *J. Am. Chem. Soc.*, 2009, **131**, 12892–12893.

18 (a) W. Huang, Q. Liu, L. Zheng and Z. Zhang, *Catal. Lett.*, 2011, **141**, 191–197; (b) P. Melchiorre, *Angew. Chem. Int. Ed.*, 2012, **51**, 9748–9770; (c) J. Duan and P. Li, *Catal. Sci. Technol.*, 2014, **3**, 311–320; (d) J. Zhou, X. Ma, J. Wan and W. Wang, *Org. Biomol. Chem.*, 2012, **10**, 4179–4185; (e) P. Czarnecki, A. Plutecka, J. Gawroński and K. Kacprzak, *Green Chem.*, 2011, **13**, 1280–1287; (f) P. Li, S. Chan, A. S. C. Chan and F. Y. Kwong, *Adv. Synth. Catal.*, 2011, **353**, 1179–1184; (g) L. Xu, J. Luo and Y. Lu, *Chem. Commun.*, 2009, **14**, 1807–1821; (h) B. Zheng, Q. Liu, C. Guo, X. Wang and L. He, *Org. Biomol. Chem.*, 2007, **5**, 2913–2915.